JACS
JOURNAL OF THE AMERICAN CHEMICAL SOCIETY
pubs.acs.org/JACS
Article

On−Off Switching of a Photocatalytic Overall Reaction through Dynamic Spin-State Transition in a Hofmann Clathrate System

Guo-Zhang Huang,[‡] Yuan-Sheng Xia,[‡] Feng Yang, Wei-Jian Long, Jing-Jing Liu, Jia-Peng Liao, Mi Zhang, Jiang Liu,* and Ya-Qian Lan*

Cite This: https://doi.org/10.1021/jacs.3c09513

Read Online

ACCESS | Metrics & More | Article Recommendations | Supporting Information

ABSTRACT: Spin-state transition is a vital factor that dominates catalytic processes, but unveiling its mechanism still faces the great challenge of the lack of catalyst model systems. Herein, we propose that the {Fe-Pt} Hofmann clathrates, whose dynamic spin-state transition of metal centers can be chemically manipulated through iodine treatment, can serve as model systems in the spin-related structural−catalytic relationship study. Taking the photocatalytic synthesis of H_2O_2 as the basic catalytic reaction, when the spin state of Fe(II) in the clathrate is high spin (HS), sacrificial agents are indispensable to the photosynthesis of H_2O_2 because only the photocatalytic oxygen reduction reaction (ORR) occurs; when it is low spin (LS), both the ORR and water oxidation reaction (WOR) can take place, enabling a high H_2O_2 photosynthesis rate of 66 000 μM g^{-1} h^{-1} under visible-light irradiation. In situ characterizations combined with density functional theory calculations confirmed that, compared with the HS-state counterpart, the LS state can induce strong charge transfer between the LS Fe(II) and the iodide-coordinating Pt(IV) in the polymer and reduce the energy barriers for both the ORR and WOR processes, dominating the on−off switching upon the photosynthesis of H_2O_2 in O_2-saturated water. What's more, the one-pot tandem reactions were conducted to utilize the synthesized H_2O_2 for transforming the low-value-added sodium alkenesulfonates into value-added bromohydrin products with decent conversion rates. This work provides a pioneering investigation into on−off switching the photocatalytic overall reaction through manipulating the metallic spin-state transition in spin-crossover systems.

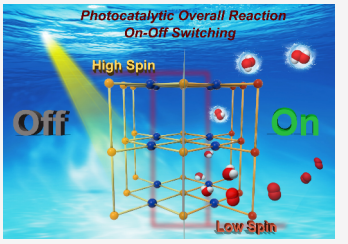

INTRODUCTION

Photocatalysis has been recognized as one of the best strategies to relieve the energy crisis and environmental pollution via solar-to-chemical energy conversion.[1−3] The catalytic efficiency of photocatalysts is governed by several key factors, such as their light-harvesting ability, the substrate adsorption and activation energies, the separation and transport of photogenerated carriers, etc.[3−6] As the intrinsic electronic characteristic of transition-metal centers, spin state has always been regarded as one of the vital factors dominating catalytic behavior through the regulation of energy levels and electronic structures.[7−10] Over the past few decades, tremendous efforts have been made to clarify the role electronic spin plays in the triplet-oxygen-involved catalytic process, but opinions vary. For instance, it has been reported that spin selection might be an effective way to promote the catalytic oxygen evolution reaction (OER) through spin polarization of the active sites, whereas it has also been reported that excess aggregation of spin carriers on the catalyst surface would rather hinder the OER.[11−15] This has raised the research topic of developing suitable model systems for exploring structural−catalytic relationships, which are strongly related to electronic spin.

There are mainly two reasons for the difficulties in uncovering such structural−catalytic relationships: (1) precisely controlling the spin states without changing the coordination structures or metallic valences of the catalysts is challenging[7,14] and (2) the spin states of the active catalytic metal sites might change during the substrate absorption and desorption processes.[13,16] With regard to overcoming the above obstacles, spin-crossover (SCO) materials might provide a perfect connatural platform, as SCO materials can exhibit reversible spin-state transitions in the presence of external chemical or physical stimuli, including guest, temperature, pressure, and light irradiation.[17−20] Fe(II) compounds with an FeN_6 octahedral coordination environment are the most studied SCO systems; their 3d-orbital electronic configurations experience a $t_{2g}^6e_g^0$ ($^1A_1$) to $t_{2g}^4e_g^2$ ($^5T_2$) transformation during the SCO process.[21] The spin transition results in significant changes in Fe−N bond lengths, photon-harvesting abilities, charge-transfer characteristics, etc., ensuring the corresponding relations between physical characteristics and catalytic performance can be linked to the spin states.

Generally, the metallic centers in conjunction with their coordination ligands would act as the energy- and electron-transfer components or active catalytic sites in the photo-

Received: August 31, 2023
Revised: November 12, 2023
Accepted: November 14, 2023

Downloaded via BEIHANG UNIV on December 11, 2023 at 02:16:42 (UTC).
See https://pubs.acs.org/sharingguidelines for options on how to legitimately share published articles.

Scheme 1. Schematic Illustrations of the Dynamic Spin-State Transition for Fe(II) in the Hofmann Clathrates and the Spin-Related Photocatalytic H_2O_2 Synthesis Overall Reaction

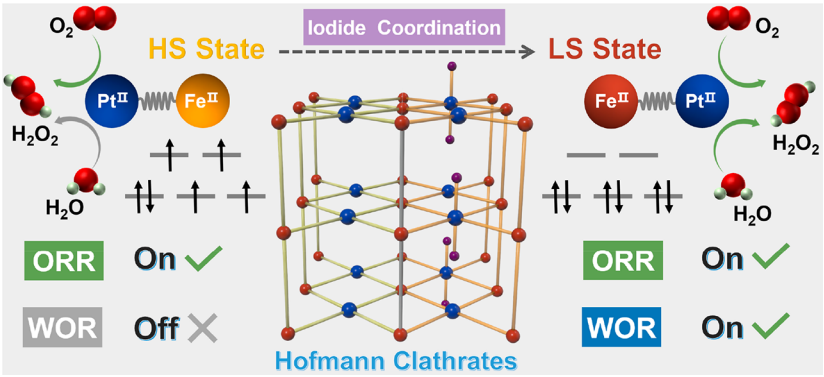

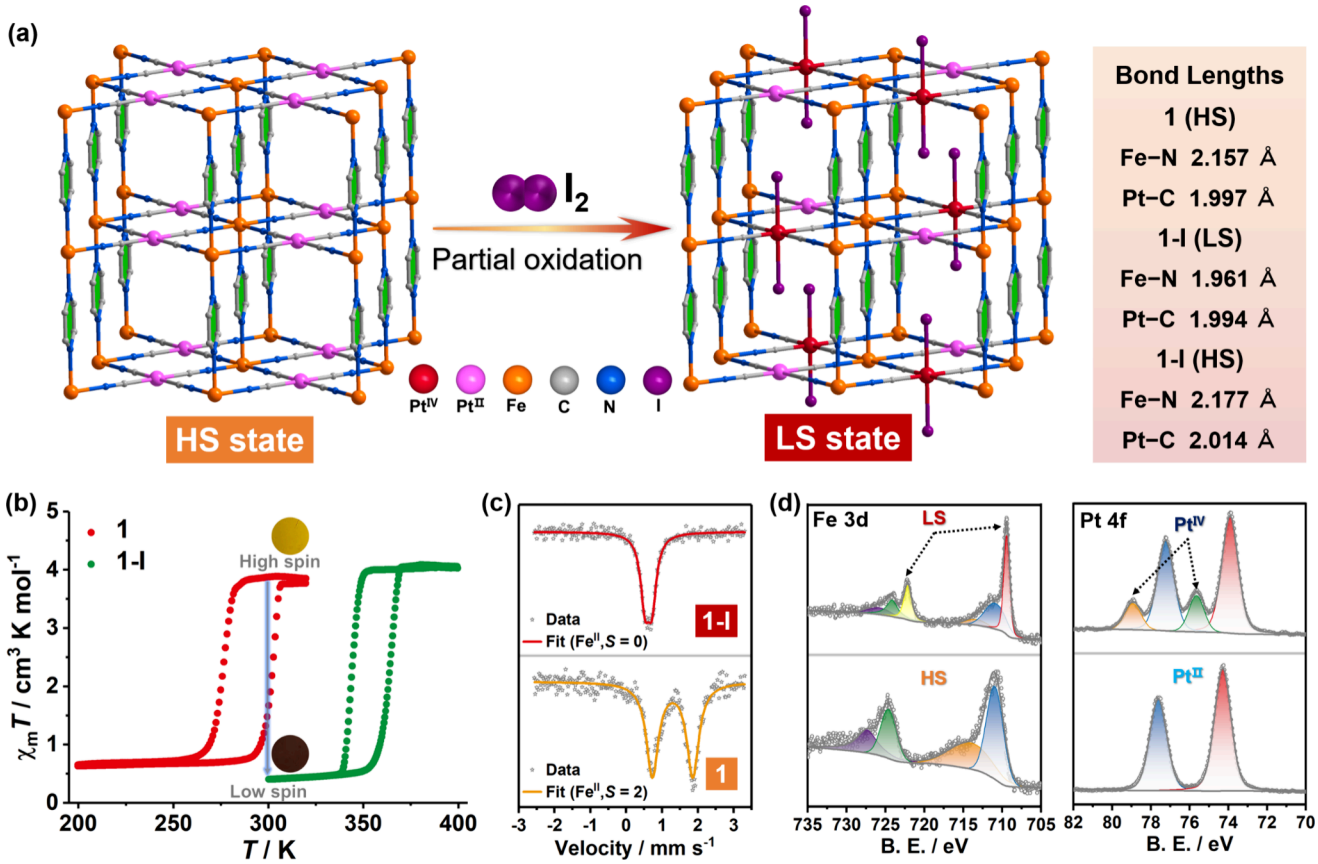

Figure 1. (a) 3D framework in the crystal structures of **1** and **1-I** and their transformation. (b) Thermally induced magnetic bistabilities in $\chi_m T$ curves and the powder colors of synthesized **1** and **1-I**. (c) ^{57}Fe Mössbauer spectra of **1** and **1-I** at room temperature. (d) Fe 3d and Pt 4f XPS spectra of **1** (bottom) and **1-I** (top) and the spin- and valence-state assignments.

catalysts separately or simultaneously. The Hofmann clathrates constructed with divalent metal ions, nitrogen-bearing ligands, and polycyanometallate linkers are well applied to obtain Fe(II) SCO systems in which the spin transition centers and the open metallic sites are separated. In this regard, SCO coordination polymers provide opportunities for investigating the spin-related energy and electron transfer during the catalytic process, rarely addressed in the past.[22−27] Herein, we demonstrate the significance for the prototypical 3D Hofmann-type coordination polymers, namely $\{Fe(Pz)[Pt^{II}(CN)_4]\}\cdot 2H_2O$ (**1**) and $\{TM(Pz)[Pt^{II}(CN)_4]_{1-x}[Pt^{IV}(CN)_4I_2]_x\}\cdot x$Solv (TM = Fe (**1-I**), x = 0.6; TM = Co (**2-I**), x = 0.5), and the dynamic spin-state transition behavior of Fe(II) from high spin (HS) to low spin (LS) by means of iodine coordination to Pt(II).[24,25] Through comprehensive characterizations and analyses, it is confirmed that the diamagnetic LS-state Fe(II) in the polymers can bring better light-harvesting ability, photogenerated carrier separation efficiency, and charge transport capacity compared with the HS-state counterpart. Furthermore, the spin alteration realized the on−off switching of the H_2O_2 photosynthesis in pure water by oxygen reduction reaction (ORR) and water oxidation reaction (WOR) (Scheme 1). In addition, theoretical calculations conducted on different spin states revealed that the LS-state Fe(II) can reduce the energy barriers of both ORR and WOR and meanwhile increase the metal−metal charge-

https://doi.org/10.1021/jacs.3c09513
J. Am. Chem. Soc. XXXX, XXX, XXX−XXX

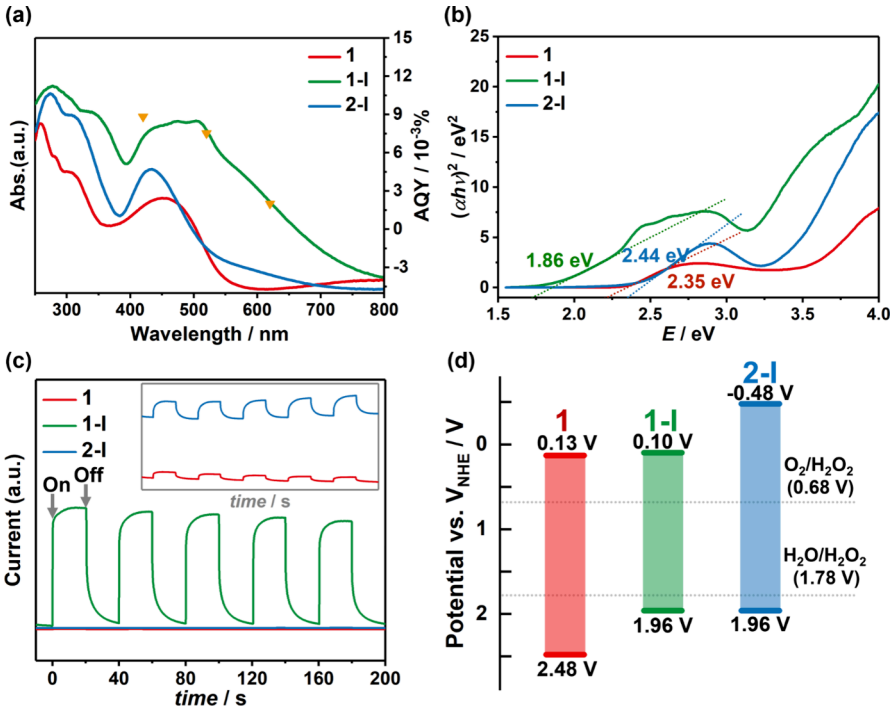

Figure 2. (a) UV−vis DRS for **1**, **1-I**, and **2-I**. The yellow triangles represent the apparent quantum yield of the H_2O_2 production for **1-I**. (b) Tauc plots for HOMO−LUMO gap calculations. (c) Transient photocurrent response. (d) Energy levels diagram.

transfer degree to increase the overall carrier transport capacity of the 3D framework. This work carves out a new avenue for investigating the spin-related structural−catalytic relationships for crystalline photocatalysts.

RESULTS AND DISCUSSION

Synthesis and Characterization. The Hofmann clathrates $\{Fe(Pz)[Pt^{II}(CN)_4]\}\cdot 2H_2O$ (**1**) have been widely studied as a prototype of chemo-responsive spin-state-switchable systems.[19] In the structure of **1**, a 3D pillared-layer-type porous framework consisting of cyano-bridged Fe^{II}−Pt^{II} layers and Pz pillar ligands was formed in which the four-coordinated Pt(II) centers can perform as open-metal sites to interact strongly with π-donor molecules. The Pt(II) atoms showed square-planar coordination geometry, while the Fe atoms were octahedrally coordinated. When an oxidative addition reaction involving excess iodine molecules was conducted on **1**, $\{Fe(Pz)[Pt^{II/IV}(CN)_4]I_{1.2}\}\cdot 2H_2O$ (**1-I**), with a similar structure to **1**, was obtained, along with half of the Pt(II) transforming into Pt(IV).[25] The axial positions of Pt(IV) in **1-I** are occupied by two iodide anions, which makes the holes and iodide atoms uniform in the crystal (Figure 1a). The average Fe−N bond length is 2.157 Å for **1** and 1.961 Å for **1-I**, indicating HS state and LS state at room temperature for **1** and **1-I**, respectively. The samples of **1** and **1-I** were prepared, according to the literature, by a one-pot reaction at room temperature, resulting in orange-yellow and dark-red powders, respectively.[22,24,25] When the Fe(II) salt was replaced with a Co(II) salt, a brown-yellow powder of **2-I** was formed, formulating as $\{Co(Pz)[Pt^{II/IV}(CN)_4]I\}\cdot H_2O\cdot 0.5CH_3OH$.[28] The phase purities of the as-prepared samples for these compounds were confirmed by powder X-ray diffraction (PXRD) measurements at room temperature, showing satisfactory results in the PXRD patterns (Figures S1−S3). Furthermore, the spin transition behaviors for **1** and **1-I** were explored by variable-temperature magnetic susceptibility measurements. As shown in the plots depicting thermal dependence $\chi_m T$ (Figure 1b), the Fe(II) ions in **1** were present in the HS state and showed a hysteresis loop with critical temperatures of T^{up} = 302 K and T^{down} = 276 K, while the Fe(II) ions in **1-I** were in the LS state, showing hysteresis loops with critical temperatures of T^{up} = 364 K and T^{down} = 344 K. When it came to **2-I**, $\chi_m T$ reached a value of 2.9 cm^3 K mol^{-1} at room temperature, revealing the HS state for the Co sites, and no spin transition happened within the 10−300 K temperature region (Figure S6). The room-temperature spin state of Fe(II) was also proven by employing ^{57}Fe Mössbauer spectroscopy. The ^{57}Fe Mössbauer spectrum of **1** showed one doublet with the values of the isomer shift (δ) and quadrupole splitting (ΔE_Q) lying in the intervals expected for Fe(II) in a HS (S = 2) state. The ^{57}Fe Mössbauer spectrum of **1-I** showed one doublet with δ and ΔE_Q values typical for Fe(II) in the LS (S = 0) state (Figure 1c and Table S2). These results were in good agreement with the crystal structures and the magnetic susceptibility measurements.

X-ray photoelectron spectroscopy (XPS) measurements were conducted to examine the valence state of the Pt centers and the spin state of Fe ions as well (Figure 1d). **1** displayed $4f_{7/2}$, $4f_{5/2}$ doublets with binding energies (BEs) of approximately 74.3 and 77.6 eV, respectively. The $4f_{7/2}$ BE was close to that found for the parent $K_2[Pt(CN)_4]$ (BE($4f_{7/2}$) = 73.8 eV), verifying the bivalence state of the Pt centers. Pt 4f spectra measured in compound **1-I** showed remarkable shoulder peaks at higher energies, evidencing the two types of Pt 4f doublets. The BEs of approximately 73.9 and 77.2 eV for the first doublet were close to those in **1**, attributed to a Pt(II) site. The second doublet, shifted to higher energies by around 1.7 eV, indicated the presence of Pt(IV) sites. The BE of approximately 75.6 eV was markedly smaller than that found for the reference $K_2[Pt^{IV}(CN)_4(Cl)_2]\cdot 3H_2O$ with BE($4f_{7/2}$) = 76.6 eV. Generally, decreases of the BEs can be attributed to

https://doi.org/10.1021/jacs.3c09513
J. Am. Chem. Soc. XXXX, XXX, XXX−XXX

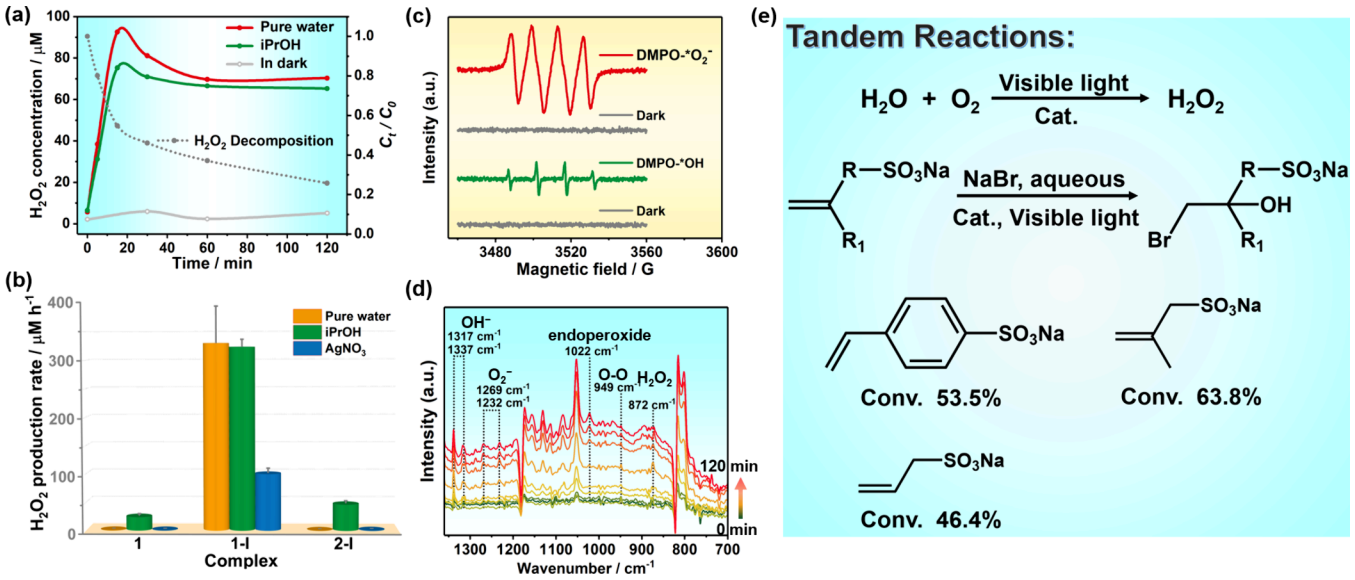

Figure 3. (a) Photocatalytic activity of **1-I** for H_2O_2 production in different reaction conditions and the H_2O_2 (500 μM) decomposition over **1-I** in dark conditions. (b) The related H_2O_2 production rates under visible-light irradiation (λ > 420 nm) using 5 mg of catalysts **1**, **1-I**, and **2-I**. (c) EPR spectrum of the reaction solution under dark and visible-light illumination in the presence of DMPO as the spin-trapping reagent. (d) In situ DRIFT spectrum of **1-I** in the H_2O_2 photosynthesis. (e) Photocatalytic oxidation of substituted NaAS into bromohydrin.

the coordinating electron donor ligands. So this may be caused by the Fe^{II}–NC–Pt^{IV} interaction in **1-I**, which means, more precisely, π back-bonding donation from the Fe(II) ion to the $[Pt^{IV}(CN)_4I_2]^{2-}$ group.[29] Due to the capacity reduction of Pt(IV) to Pt(II) with the soft X-ray photons, the amount of Pt(IV) would decrease as irradiation time increased, thus hindering the estimation of the Pt(II):Pt(IV) ratio. Furthermore, the XPS results were sensitive to the changes of the Fe(II) spin state in the meantime. **1** displayed $2p_{3/2}$, $2p_{1/2}$ doublets with BEs of approximately 711.0 and 724.6 eV, respectively. Two broad shakeup satellite peaks emerged at about 4.0 and 3.8 eV beyond the $2p_{3/2}$ and $2p_{1/2}$ bands. Both the appearance of the broad $2p_{3/2}$ and $2p_{1/2}$ bands and the prominent satellite peaks revealed the presence of the paramagnetic state for the Fe(II) centers, namely, the HS state. When referring to **1-I**, owing to the reduction activation of Pt(IV) with the X-ray photons, the Fe 2p XPS spectra were more complicated, their deconvolution showing six peaks in total. Two $2p_{3/2}$ and $2p_{1/2}$ peaks and two satellite peaks among those peaks corresponded to the HS Fe(II) sites, and the other two components, showing narrow peak shapes with dominating intensity, were the $2p_{3/2}$ and $2p_{1/2}$ peaks of LS-state Fe(II) ions. The BEs associated with each component are shown in Tables S3–S5.

The dynamic transition of spin states for the metallic sites could exert a significant impact on the electronic energy level as well as the charge transport capacity of the 3D polymers. In the first place, UV–vis diffuse reflectance spectra (DRS) were obtained to investigate the photon capture ability of the compounds here. As seen in Figure 2a, all compounds showed light absorption in the visible region. In **1**, the poorest visible-light absorption resulted from the only occurrence of ligand-to-metal charge transfer (LMCT) of the HS Fe(II) centers. The presence of Pt^{IV}–I in **2-I** did not significantly enhance its light-harvesting ability comparing to **1**. Nevertheless, **1-I** exhibited a much better light-harvesting ability in the visible-light region, mainly on account of the charge-transfer band from LS Fe^{II} to Pt(IV). By analyzing the Tauc plots of $(\alpha h\nu)^2$ vs photon energy, the HOMO–LUMO gaps E_g were obtained to be 2.35, 1.86, and 2.44 eV for **1**, **1-I**, and **2-I**, respectively. In order to verify the energy level positions, Mott–Schottky (M-S) electrochemical measurements were carried out. Based on the M-S results, the HOMO positions for **1**, **1-I**, and **2-I** were calculated to be 0.13, 0.10, and −0.48 eV, respectively (Figures S14–S16). On the basis of the equation $E_g = E_{LUMO} - E_{HOMO}$, the HOMO positions of **1**, **1-I**, and **2-I** were calculated with ease to be 2.48, 1.96, and 1.96 eV, respectively. As shown in Figure 2d, the energy levels of **1**, **1-I**, and **2-I** were adequate for the synthesis of H_2O_2 from H_2O ($E(H_2O_2/H_2O)$ = +1.78 V vs NHE) and O_2 ($E(O_2/H_2O_2)$ = +0.68 V vs NHE).[30]

In the second place, the transient photocurrent response and electrochemical impedance spectroscopy (EIS) were measured to evaluate the photogenerated carrier separation efficiency and charge transport capacity. As shown in Figure 2c, the photocurrent density of **1-I** was prodigiously high and had an excellent reproducibility in the process of visible-light on–off cycles, whereas **1** and **2-I** showed tiny current responses to visible-light irradiation. At the same time, the electronic conductivity of **1-I** was also superior to those of the other two species, which was proved by the smaller semicircle radius in the EIS measurements (Figure S17). All these results revealed that **1-I** had a higher charge separation efficiency, more usable surface carriers, and faster interface electron-transfer speed. As the photon capture ability and charge transport capacity of **1** and **2-I** were quite comparable, it meant that the involvement of the Pt^{IV}–I moiety did not improve the light-harvesting ability and the motion characteristics of carriers much. **1-I** performed much better in terms of those characteristics, indicating the key role of the LS-state Fe(II) centers inside the clathrates in light absorption and carrier transport.

In view of the energy level structures for the three Hofmann clathrates, we first investigated their photocatalytic activities in H_2O_2 production under visible-light (λ > 420 nm) irradiation in an O_2-saturated aqueous solution without additional sacrificial agents. First, we verified that **1** and **2-I** showed no photocatalytic activity while **1-I** demonstrated a high photo-

https://doi.org/10.1021/jacs.3c09513
J. Am. Chem. Soc. XXXX, XXX, XXX–XXX

catalytic H_2O_2 production activity. The optimum catalyst concentration experiment revealed that about 1 mg of **1-I** per mL of water can give the best rate for photosynthetic production of H_2O_2 (Figure S20). For as-prepared **1-I**, there were a clear accumulation of the H_2O_2 yield for a while, and the photosynthetic rate would decrease with increasing irradiation time (Figure 3a). This is because the generated H_2O_2 react with the photoinduced electrons or holes of the photocatalysts, resulting in the continuous decomposition simultaneously decomposed on Pt^{II} sites.[31] The optimized photosynthetic rate of H_2O_2 in pure water for **1-I** reached 330 $\mu M\ h^{-1}$, which surpassed those of a lot of previous crystalline coordination photocatalysts.[32] After irradiation for more than 1 h, the H_2O_2 concentration remained steady, meaning that the photoproduction rate of H_2O_2 is comparable with its decomposition rate, the value of which was close to 70 $\mu M\ h^{-1}$. Furthermore, with Ar bubbling for 30 min to eliminate O_2 or in the dark, **1-I** displayed almost no H_2O_2 yield, demonstrating the indispensable role that photocatalysis of O_2 plays in the reaction (Figure 3b). The apparent quantum yields (AQYs) under different wavelength monochromatic illumination were $(6.0-26) \times 10^{-3}$ % (420−620 nm) for **1-I**, which are in agreement with the optical properties (Figure 2a). Cycling stability tests were also carried out to evaluate the durability of the photocatalyst in this system. After four cycles of photocatalytic tests, the catalytic performance showed a decrease and the H_2O_2 yield dropped to 177 $\mu M\ h^{-1}$ (Figure S21). The PXRD patterns after photocatalysis suggested the structural integrity and no significant loss of the crystallinity for the catalysts. What's more, the XPS spectra before and after the reaction were compared and the BEs of the metallic centers remained unchanged, which means the valence states as well as the spin states for Fe and Pt sites are retained (Figures S8−S13).

Generally, the photosynthesis formation of H_2O_2 had two possible pathways: the two-electron ORR and the two-electron WOR.[32−34] To investigate the mechanisms of the distinctly different photocatalytic H_2O_2 production processes with the synthesized SCO clathrates, a series of control experiments were carried out. First, photocatalytic ORR for H_2O_2 production using isopropanol (iPrOH) as a sacrificial reagent was evaluated in an O_2-saturated 10% iPrOH aqueous solution. Experimental results showed variable photocatalytic activities with photosynthetic rates of H_2O_2 of 24, 323, and 46 $\mu M\ h^{-1}$ for **1**, **1-I**, and **2-I**, respectively. Then, the photocatalytic WOR for H_2O_2 production was studied with Ar in $AgNO_3$ aqueous solution. Only **1-I** was detected to show photocatalytic activity, with a H_2O_2 photosynthetic rate of 100 $\mu M\ h^{-1}$, and almost no dioxygen was be detected under these conditions. Moreover, an isotopic experiment to simulate the real system (without $AgNO_3$) was conducted for **1-I** to verify the as-proposed mechanism of the ORR by using $^{18}O_2$ (as an electron acceptor) and $H_2{}^{16}O$ (as an electron donor). $^{18}O_2$ (m/z = 36) could be detected in the decomposition product of the reaction between photogenerated H_2O_2 and MnO_2 (Figure S23), indicating the H_2O_2 photosynthesis process from ORR. The above results reveal that (i) **1** and **2-I** exhibited only photocatalytic ORR activity, whereas **1-I** can exhibit both photocatalytic WOR and ORR activity for H_2O_2 production, and (ii) the ORR photocatalytic activity was higher for **1-I** than for **1** and **2-I**. Preliminarily, we can deduce that (i) the LS-state Fe(II) in the Fe−Pt clathrates switches "on" the H_2O_2 photosynthesis overall reaction, while (ii) the HS-state metallic center, whether Fe(II) or Co(II), would switch "off" such a reaction. Seemingly, the difference in the photocatalytic activity of the ORR half-reaction might be caused by the light absorption ability and carrier transport capacity, but further investigations are needed to understand the on−off switching of the overall photoreaction.

As for the H_2O_2 photosynthesis reaction routes, there were two possible routes for ORR and for WOR from O_2 and water, respectively, via the $2e^-$ redox process. One of them was a $2e^-$ two-step process with hydroxyl radicals ($^{\bullet}OH$) and superoxide anion radicals ($^{\bullet}O_2^-$) as the intermediate species for indirect H_2O_2 generation, and the other one was a direct $2e^-$ one-step process.[35−37] In order to verify the mechanism of the full H_2O_2 photosynthesis reaction, electron paramagnetic resonance (EPR) spectroscopy was conducted using 5,5-dimethyl-pyrroline *N*-oxide (DMPO) as the free-radical spin-trapping agent to detect $^{\bullet}OH$ and $^{\bullet}O_2^-$. On one hand, there was no EPR signal observed for **1** in O_2-saturated water under dark and visible-light illumination (Figure S22). On the other hand, typical characteristic EPR signals of the DMPO−$^{\bullet}O_2^-$ species and the DMPO−$^{\bullet}OH$ species were observed for **1-I** under visible-light irradiation in O_2-saturated water and in Ar-protected $AgNO_3$ aqueous solution, respectively, which would both be absent in dark conditions (Figure 3c). These findings implied that the H_2O_2 photosynthesis reaction with **1-I** went through a $2e^-$ two-step process with the participation of $^{\bullet}OH$ and $^{\bullet}O_2^-$.

In situ diffuse reflectance infrared Fourier transform spectroscopy (in situ DRIFTs) is another powerful tool for understanding the reaction mechanisms in H_2O_2 photosynthesis. When a sample of **1** was irradiated in moist oxygen, the infrared absorptions were quite steady, showing thermal effects only on the IR absorptions of Fe−CN (2140−2220 cm^{-1} region) and the pyrazine rings (780−832 and 1030−1200 cm^{-1} regions) (Figure S24). When **1-I** was used in darkness, it displayed relatively weak infrared absorption peaks at room temperature. Before the sample was blown with moist oxygen and irradiated, the infrared absorptions corresponding to the Fe−CN and the pyrazine rings showed dramatic changes during the thermal activation process, due to the spin transition of the Fe(II) and the photoexcitation (Figure S25). After the system was equilibrated in moist O_2, the sample was irradiated with visible light, and IR peaks emerged gradually at 949, 1022, and 1232 cm^{-1} which are attributed to the O−O bonding, the endoperoxide intermediate, and the $^*O_2^-$ species, respectively.[38] Meanwhile, the infrared absorptions of $^*OH^-$ located 1317 and 1337 cm^{-1} also showed increasing intensity, which implied the dehydrogenation of H_2O molecules under irradiation.[39] In addition, the signal of H_2O_2 located at 872 cm^{-1} was observed as well (Figure 3d).[40]

Based on the above experimental results, a possible mechanism can be proposed to illustrate the visible-light-driven photosynthesis of H_2O_2. Referring to compound **1-I**, the dioxygen was absorbed and gained electrons at the Pt(II) sites to generate the $^{\bullet}O_2^-$ active intermediate; meanwhile, the H_2O molecule turned into $^{\bullet}OH$ after using the holes. Subsequently, proton transfer and electron transfer continually took place on the $^{\bullet}O_2^-$, producing $^{\bullet}OOH$ and then forming H_2O_2. After that, two $^{\bullet}OH$'s were desorbed from the Pt(II) sites to transform into H_2O_2 as well. To clarify the spin-related photocatalytic mechanism from a microscopic point of view, temperature-programmed desorption (TPD) of O_2 and H_2O was carried out for **1** and **1-I**. The results of the equations of

https://doi.org/10.1021/jacs.3c09513
J. Am. Chem. Soc. XXXX, XXX, XXX−XXX

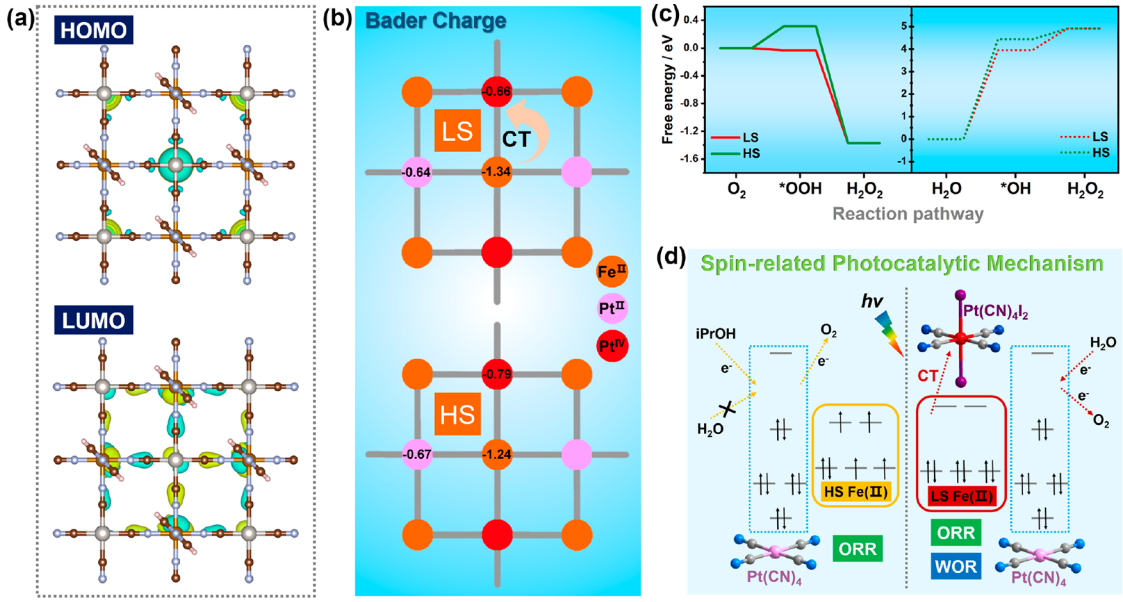

Figure 4. (a) Distribution of HOMO and LUMO wave functions of the LS-state **1-I** in real space. (b) Bader charge analysis of **1-I** in the LS and HS states. The black numbers at the atomic center are the Bader charge of the respective atom. (c) Free energy diagram of **1-I** in LS and HS states for photosynthesis of H_2O_2 through the ORR (full line) and WOR (break line) pathways. (d) The spin-related proposed reaction mechanisms.

the O_2-TPD and H_2O-TPD revealed that the active interaction between molecular O_2/H_2O and the Pt(II) sites was stronger in the LS state than in the HS state (Figure S26).

To understand further how the dynamic spin-state transition behavior of Fe(II) in the Hofmann clathrate manipulates the catalytic performance, density functional theory (DFT) calculations were conducted on **1-I** at its HS and LS states, respectively. The theoretical calculations analyzing the contributions of molecular orbitals revealed quite similar spatial charge separation for both spin states (Figure 4a and Figure S30). As a result, we carried out a Bader charge analysis to further uncover the electronic differences between the HS- and LS-state Hofmann polymers. As shown in Figure 4b, the Bader charge values of Pt(II) are close for different spin states, while a more negative value for Fe(II) and a more positive value for Pt(IV) were observed in the LS-state structure. This result directly shows that significant Fe(II)−Pt(IV) charge transfer exists in the LS clathrate, in agreement with the foregoing experimental results. Besides the molecular orbital and the charge calculations, we also conducted theoretical investigations of the ORR and WOR processes for HS and LS structures, respectively. The calculation results showed that both dioxygen and water molecules were chemically absorbed on the Pt(II) sites via the formation of Pt−O bonds. As for dioxygen absorption, the Pt−O bond lengths are 2.36 Å for the LS-state structure and 2.28 Å for the HS-state structure, i.e., shorter for the latter. The Pt−O bond lengths between H_2O and Pt(II) are 2.08 Å for the LS-state structure and 2.06 Å for the HS-state structure, which are comparable. These results indicate that chemical absorption of the O_2 and H_2O molecules can occur easily on the open site Pt(II), facilitating the ORR and WOR to proceed through the photoinduced electron and hole transfer from adsorption sites to the substrates.

Although slightly shorter Pt−O bond lengths are observed between substrates and Pt(II) for the HS-state structure in the DFT calculation results, the redox reaction free energies of O_2 and H_2O on Pt(II) sites are lower for the LS-state structure compared with the HS-state structure. Generally, the processes from O_2 to $^{\bullet}$OOH intermediate and from H_2O to $^{\bullet}$OH intermediate are the rate-determining steps for the photocatalytic H_2O_2 production. As shown in Figure 4c, the free energies of one-electron reduction and hydrogenation for the O_2 molecule are −0.04 eV for the LS-state structure and 0.31 eV for the HS-state structure. Similarly, the free energies of one-electron oxidation and dehydrogenation for the H_2O molecule are 3.95 eV for the LS-state structure and 4.44 eV for the HS-state structure. Hence, combining the experimental results and the theoretical calculations, we can finally get some insights into how the spin states of Fe(II) in the Fe−Pt clathrates affect the photocatalytic overall reaction. To sum up, the excellent light-harvesting ability as well as the higher carrier transport capacity of **1-I** compared with **1** and **2-I** mainly result from the charge transfer between the LS Fe(II) and Pt(IV) sites. This enhances the ORR photocatalytic activity of **1-I** and gives a much higher yield of the photosynthesized H_2O_2. Further, the redox reaction energy barriers are lower in the LS-state structures, making a contribution to the overall photosynthesis of H_2O_2 here.

So far, due to the severe decomposition of H_2O_2 on photocatalyst **1-I**, we try to utilize the photosynthesized H_2O_2 in a one-pot reaction system to produce value-added chemicals. To this point, several water-soluble alkenes, including sodium alkenesulfonate (NaAS), were selected as the substrates to investigate the value-added photochemical reaction. By adding NaBr as another reagent, NaAS substrates can be oxidated into bromohydrin products with good conversion rates in pure water with **1-I** as the photocatalyst under visible-light irradiation (Figure 3e and Figures S27−S29).

CONCLUSIONS

In summary, we have demonstrated the spin-crossover Hofmann clathrates to be ideal model catalyst systems for investigating spin-related structural−catalytic relationships for the first time. The dynamic spin-state transition in the

https://doi.org/10.1021/jacs.3c09513
J. Am. Chem. Soc. XXXX, XXX, XXX−XXX

clathrates enables them to be applied to the switching "on" and "off" for the photocatalytic overall reaction leading to H_2O_2 production. When the Fe(II) in the Fe−Pt polymer stays at the high-spin state, only photocatalytic ORR can take place, and the photosynthesis of H_2O_2 fails to occur in pure water. In contrast, when the spin state of Fe(II) is tuned to low spin, both ORR and WOR can happen, enabling the photosynthesis of H_2O_2 from O_2 and H_2O. The theoretical calculations combined with in situ measurements revealed that the increase of charge-transfer degree between the Fe(II) and Pt(IV) sites in the LS-state clathrate brings better light-harvesting ability and carrier transport capacity, resulting in a photocatalytic activity enhancement. Moreover, both the reducing of energy barriers via the ORR and WOR processes and the strengthening of the substrate−catalyst interaction in the LS-state structure play key roles in the switching on−off of the photocatalytic overall reaction. In addition, the H_2O_2 can be utilized in a one-pot tandem reaction to transform sodium alkene sulfonate into its value-added bromohydrin products. This work opens opportunities for building up new model catalyst systems for further exploration of the spin-related structural−catalytic relationship as well as for unmasking a spin-driven catalytic mechanism.

■ ASSOCIATED CONTENT

Supporting Information

The Supporting Information is available free of charge at https://pubs.acs.org/doi/10.1021/jacs.3c09513.

Detailed information regarding the experimental methods, characterization analysis, and DFT calculations (PDF)

■ AUTHOR INFORMATION

Corresponding Authors

Ya-Qian Lan − *National and Local Joint Engineering Research Center of MPTES in High Energy and Safety LIBs, Engineering Research Center of MTEES (Ministry of Education), and Key Laboratory of ETESPG (GHEI), School of Chemistry, South China Normal University, Guangzhou 510006, China;* orcid.org/0000-0002-2140-7980; Email: yqlan@m.scnu.edu.cn

Jiang Liu − *National and Local Joint Engineering Research Center of MPTES in High Energy and Safety LIBs, Engineering Research Center of MTEES (Ministry of Education), and Key Laboratory of ETESPG (GHEI), School of Chemistry, South China Normal University, Guangzhou 510006, China;* orcid.org/0000-0002-2596-4928; Email: liuj0828@m.scnu.edu.cn

Authors

Guo-Zhang Huang − *Department of Chemistry, Guangdong Provincial Key Laboratory of Catalytic Chemistry, Southern University of Science and Technology, Shenzhen, Guangdong 518055, China;* orcid.org/0000-0001-9167-0090

Yuan-Sheng Xia − *National and Local Joint Engineering Research Center of MPTES in High Energy and Safety LIBs, Engineering Research Center of MTEES (Ministry of Education), and Key Laboratory of ETESPG (GHEI), School of Chemistry, South China Normal University, Guangzhou 510006, China*

Feng Yang − *Department of Chemistry, Guangdong Provincial Key Laboratory of Catalytic Chemistry, Southern University of Science and Technology, Shenzhen, Guangdong 518055, China;* orcid.org/0000-0002-3637-814X

Wei-Jian Long − *National and Local Joint Engineering Research Center of MPTES in High Energy and Safety LIBs, Engineering Research Center of MTEES (Ministry of Education), and Key Laboratory of ETESPG (GHEI), School of Chemistry, South China Normal University, Guangzhou 510006, China*

Jing-Jing Liu − *National and Local Joint Engineering Research Center of MPTES in High Energy and Safety LIBs, Engineering Research Center of MTEES (Ministry of Education), and Key Laboratory of ETESPG (GHEI), School of Chemistry, South China Normal University, Guangzhou 510006, China*

Jia-Peng Liao − *National and Local Joint Engineering Research Center of MPTES in High Energy and Safety LIBs, Engineering Research Center of MTEES (Ministry of Education), and Key Laboratory of ETESPG (GHEI), School of Chemistry, South China Normal University, Guangzhou 510006, China*

Mi Zhang − *National and Local Joint Engineering Research Center of MPTES in High Energy and Safety LIBs, Engineering Research Center of MTEES (Ministry of Education), and Key Laboratory of ETESPG (GHEI), School of Chemistry, South China Normal University, Guangzhou 510006, China*

Complete contact information is available at: https://pubs.acs.org/10.1021/jacs.3c09513

Author Contributions

‡G.-Z.H. and Y.-S.X. contributed equally to this work.

Notes

The authors declare no competing financial interest.

■ ACKNOWLEDGMENTS

This study was financially supported by the NSFC (Grants nos. 22225109 and 22271104), the Top Youth Project of Guangdong Pearl River Talents Program (No. 2021QN02L617), and the Open Subject Project of Key Laboratory of Bioinorganic and Synthetic Chemistry (Sun Yat-sen University).

■ REFERENCES

(1) Hoffmann, M. R.; Martin, S. T.; Choi, W.; Bahnemann, D. W. Environmental applications of semiconductor photocatalysis. *Chem. Rev.* **1995**, *95*, 69−96.

(2) Fang, Y.; Ma, Y.; Zheng, M.; Yang, P.; Asiri, A. M.; Wang, X. Metal−organic frameworks for solar energy conversion by photoredox catalysis. *Coord. Chem. Rev.* **2018**, *373*, 83−115.

(3) Zhang, B.; Sun, L. Artificial photosynthesis: opportunities and challenges of molecular catalysts. *Chem. Soc. Rev.* **2019**, *48*, 2216−2264.

(4) Chang, X.; Wang, T.; Gong, J. CO_2 photo-reduction: insights into CO_2 activation and reaction on surfaces of photocatalysts. *Energy Environ. Sci.* **2016**, *9*, 2177−2196.

(5) Wang, Z.; Li, C.; Domen, K. Recent developments in heterogeneous photocatalysts for solar-driven overall water splitting. *Chem. Soc. Rev.* **2019**, *48*, 2109−2125.

(6) Xu, S.; Carter, E. A. Theoretical insights into heterogeneous photo-electrochemical CO_2 reduction. *Chem. Rev.* **2019**, *119*, 6631−6669.

(7) Gong, Y.-N.; Zhong, W.; Li, Y.; Qiu, Y.; Zheng, L.; Jiang, J.; Jiang, H.-L. Regulating photocatalysis by spin-state manipulation of

cobalt in covalent organic frameworks. *J. Am. Chem. Soc.* **2020**, *142*, 16723−16731.
(8) Cao, A.; Bukas, V. J.; Shadravan, V.; Wang, Z.; Li, H.; Kibsgaard, J.; Chorkendorff, I.; Norskov, J. K. A spin promotion effect in catalytic ammonia synthesis. *Nat. Commun.* **2022**, *13*, 2382.
(9) Lin, C.-C.; Liu, T.-R.; Lin, S.-R.; Boopathi, K. M.; Chiang, C.-H.; Tzeng, W.-Y.; Chien, W.-C.; Hsu, H.-S.; Luo, C.-W.; Tsai, H.-Y.; Chen, H.-A.; Kuo, P.-C.; Shiue, J.; Chiou, J.-W.; Pong, W.-F.; Chen, C.-C.; Chen, C.-W. Spin-polarized photocatalytic CO_2 reduction of Mn-doped perovskite nanoplates. *J. Am. Chem. Soc.* **2022**, *144*, 15718−15726.
(10) Zhang, L.; Ren, X.; Zhao, X.; Zhu, Y.; Pang, R.; Cui, P.; Jia, Y.; Li, S.; Zhang, Z. Synergetic charge transfer and spin selection in CO oxidation at neighboring magnetic single-atom catalyst sites. *Nano Lett.* **2022**, *22*, 3744−3750.
(11) Mtangi, W.; Kiran, V.; Fontanesi, C.; Naaman, R. Role of the electron spin polarization in water splitting. *J. Phys. Chem. Lett.* **2015**, *6*, 4916−4922.
(12) Jiao, Y.; Sharpe, R.; Lim, T.; Niemantsverdriet, J. W. H.; Gracia, J. Photosystem II acts as a spin-controlled electron gate during oxygen formation and evolution. *J. Am. Chem. Soc.* **2017**, *139*, 16604−16608.
(13) Tong, Y.; Guo, Y.; Chen, P.; Liu, H.; Zhang, M.; Zhang, L.; Yan, W.; Chu, W.; Wu, C.; Xie, Y. Spin-state regulation of perovskite cobaltite to realize enhanced oxygen evolution activity. *Chem.* **2017**, *3*, 812−821.
(14) Pan, L.; Ai, M.; Huang, C.; Yin, L.; Liu, X.; Zhang, R.; Wang, S.; Jiang, Z.; Zhang, X.; Zou, J.-J.; Mi, W. Manipulating spin polarization of titanium dioxide for efficient photocatalysis. *Nat. Commun.* **2020**, *11*, 418.
(15) Li, Z.; Wang, Z.; Xi, S.; Zhao, X.; Sun, T.; Li, J.; Yu, W.; Xu, H.; Herng, T. S.; Hai, X.; Lyu, P.; Zhao, M.; Pennycook, S. J.; Ding, J.; Xiao, H.; Lu, J. Tuning the spin density of cobalt single-atom catalysts for efficient oxygen evolution. *ACS Nano* **2021**, *15*, 7105−7113.
(16) Wu, D.; Yin, H.-Q.; Wang, Z.; Zhou, M.; Yu, C.; Wu, J.; Miao, H.; Yamamoto, T.; Zhaxi, W.; Huang, Z.; Liu, L.; Huang, W.; Zhong, W.; Einaga, Y.; Jiang, J.; Zhang, Z.-M. Spin manipulation in a metal-organic layer through mechanical exfoliation for highly selective CO_2 photoreduction. *Angew. Chem., Int. Ed.* **2023**, *62*, e202301925.
(17) Gütlich, P.; Hauser, A. Thermal and light-induced spin crossover in iron(II) complexes. *Coord. Chem. Rev.* **1990**, *97*, 1−22.
(18) Gutlich, P.; Ksenofontov, V.; Gaspar, A. Pressure effect studies on spin crossover systems. *Coord. Chem. Rev.* **2005**, *249*, 1811−1829.
(19) Ni, Z.-P.; Liu, J.-L.; Hoque, M. N.; Liu, W.; Li, J.-Y.; Chen, Y.-C.; Tong, M.-L. Recent advances in guest effects on spin-crossover behavior in Hofmann-type metal-organic frameworks. *Coord. Chem. Rev.* **2017**, *335*, 28−43.
(20) Wu, S.-G.; Wang, L.-F.; Ruan, Z.-Y.; Du, S.-N.; Gomez-Coca, S.; Ni, Z.-P.; Ruiz, E.; Chen, X.-M.; Tong, M.-L. Redox-programmable spin-crossover behaviors in a cationic framework. *J. Am. Chem. Soc.* **2022**, *144*, 14888−14896.
(21) Real, J. A.; Andres, E.; Munoz, M. C.; Julve, M.; Granier, T.; Bousseksou, A.; Varret, F. Spin crossover in a catenane supramolecular system. *Science* **1995**, *268*, 265−267.
(22) Niel, V.; Martinez-Agudo, J. M.; Munoz, M. C.; Gaspar, A. B.; Real, J. A. Cooperative spin crossover behavior in cyanide-bridged Fe(II)-M(II) bimetallic 3D Hofmann-like networks (M = Ni, Pd, and Pt). *Inorg. Chem.* **2001**, *40*, 3838−3839.
(23) Boldog, I.; Gaspar, A. B.; Martinez, V.; Pardo-Ibanez, P.; Ksenofontov, V.; Bhattacharjee, A.; Gutlich, P.; Real, J. A. Spin-crossover nanocrystals with magnetic, optical, and structural bistability near room temperature. *Angew. Chem., Int. Ed.* **2008**, *47*, 6433−6437.
(24) Agustí, G.; Ohtani, R.; Yoneda, K.; Gaspar, A. B.; Ohba, M.; Sánchez-Royo, J. F.; Muñoz, M. C.; Kitagawa, S.; Real, J. A. Oxidative addition of halogens on open metal sites in a microporous spin-crossover coordination polymer. *Angew. Chem., Int. Ed.* **2009**, *48*, 8944−8947.
(25) Ohtani, R.; Yoneda, K.; Furukawa, S.; Horike, N.; Kitagawa, S.; Gaspar, A. B.; Munoz, M. C.; Real, J. A.; Ohba, M. Precise control and consecutive modulation of spin transition temperature using chemical migration in porous coordination polymers. *J. Am. Chem. Soc.* **2011**, *133*, 8600−8605.
(26) Wang, L.-F.; Wu, S.-G.; Ruan, Z.-Y.; Jian, A.-Q.; Cui, W.; Ni, Z.-P.; Tong, M.-L. A dual-switching spin-crossover framework with redox regulation and guest response. *Sci. China Chem.* **2023**, *66*, 1744−1749.
(27) Lyu, B.-H.; Ruan, Z.-Y.; Cui, W.; Wu, S.-G.; Ni, Z.-P.; Tong, M.-L. Successive redox modulation in an iron(II) spin-crossover framework. *Inorg. Chem. Front.* **2023**, *10*, 3577−3583.
(28) Pei, J.; Gu, X. W.; Liang, C. C.; Chen, B.; Li, B.; Qian, G. Robust and radiation-resistant Hofmann-type metal-organic frameworks for record xenon/krypton separation. *J. Am. Chem. Soc.* **2022**, *144*, 3200−3209.
(29) Battocchio, C.; Fratoddi, I.; Vittoria Russo, M.; Polzonetti, G. H_2S gas interaction with Pt(II)-containing polymetallaynes of selected chain length: an XPS and EXAFS study. *J. Phys. Chem. A* **2008**, *112*, 7365−7373.
(30) Kofuji, Y.; Isobe, Y.; Shiraishi, Y.; Sakamoto, H.; Tanaka, S.; Ichikawa, S.; Hirai, T. Carbon nitride-aromatic diimide-graphene nanohybrids: metal-free photocatalysts for solar-to-hydrogen peroxide energy conversion with 0.2% efficiency. *J. Am. Chem. Soc.* **2016**, *138*, 10019−10025.
(31) Wickramasinghe, L. A.; Sharp, P. R. Photoreduction of Pt(IV) halo-hydroxo complexes: possible hypohalous acid elimination. *Inorg. Chem.* **2014**, *53*, 1430−1442.
(32) Shiraishi, Y.; Takii, T.; Hagi, T.; Mori, S.; Kofuji, Y.; Kitagawa, Y.; Tanaka, S.; Ichikawa, S.; Hirai, T. Resorcinol-formaldehyde resins as metal-free semiconductor photocatalysts for solar-to-hydrogen peroxide energy conversion. *Nat. Mater.* **2019**, *18*, 985−993.
(33) Xu, J.; Zheng, X.; Feng, Z.; Lu, Z.; Zhang, Z.; Huang, W.; Li, Y.; Vuckovic, D.; Li, Y.; Dai, S.; Chen, G.; Wang, K.; Wang, H.; Chen, J. K.; Mitch, W.; Cui, Y. Organic wastewater treatment by a single-atom catalyst and electrolytically produced H_2O_2. *Nat. Sustain.* **2021**, *4*, 233−241.
(34) Chen, X.; Kondo, Y.; Li, S.; Kuwahara, Y.; Mori, K.; Zhang, D.; Louis, C.; Yamashita, H. Visible-light-driven hydrogen peroxide production from water and dioxygen by perylenetetracarboxylic diimide modified titanium-based metal−organic frameworks. *J. Mater. Chem. A* **2021**, *9*, 26371−26380.
(35) Jiang, H. Y.; Zhou, P.; Wang, Y.; Duan, R.; Chen, C.; Song, W.; Zhao, J. Copper-based coordination polymer nanostructure for visible light photocatalysis. *Adv. Mater.* **2016**, *28*, 9776−9781.
(36) Li, S.; Dong, G.; Hailili, R.; Yang, L.; Li, Y.; Wang, F.; Zeng, Y.; Wang, C. Effective photocatalytic H_2O_2 production under visible light irradiation at g-C_3N_4 modulated by carbon vacancies. *Appl. Catal. B Environ.* **2016**, *190*, 26−35.
(37) Zeng, X.; Liu, Y.; Hu, X.; Zhang, X. Photoredox catalysis over semiconductors for light-driven hydrogen peroxide production. *Green Chem.* **2021**, *23*, 1466−1494.
(38) Kou, M.; Wang, Y.; Xu, Y.; Ye, L.; Huang, Y.; Jia, B.; Li, H.; Ren, J.; Deng, Y.; Chen, J.; Zhou, Y.; Lei, K.; Wang, L.; Liu, W.; Huang, H.; Ma, T. Molecularly engineered covalent organic frameworks for hydrogen peroxide photosynthesis. *Angew. Chem., Int. Ed.* **2022**, *61*, e202200413.
(39) Yang, C.; Wan, S.; Zhu, B.; Yu, J.; Cao, S. Calcination-regulated microstructures of donor-acceptor polymers towards enhanced and stable photocatalytic H_2O_2 production in pure water. *Angew. Chem., Int. Ed.* **2022**, *61*, e202208438.
(40) Lin, W.; Frei, H. Photochemical and FT-IR probing of the active site of hydrogen peroxide in Ti silicalite sieve. *J. Am. Chem. Soc.* **2002**, *124*, 9292−9298.

https://doi.org/10.1021/jacs.3c09513
J. Am. Chem. Soc. XXXX, XXX, XXX−XXX